Structural and Optical Properties of Ag-Decorated ZnO Nanoparticles Synthesised via Hydrothermal Method for Optoelectronic Devices

[1,3]*M. I. Kimpa, [2]M. M. Kpanje, [1,2]H. Isah [1]F. M. Abdullahi, [3]A. Rashidah, [1]A. A. Abubakar, [1]Y. Titus and [1]K. U. Isah

[1]Department of Physics, School of Physical Sciences, Federal University of Technology Minna.
[2]Department of Physical Sciences, School of Natural and Applied Sciences, Niger State Polytechnic Zungeru.
[3]Department of Physics, Faculty of Sciences, Islamic University in Uganda.
***Corresponding Author:** kimpa@futminna.edu.ng (+234-803-8654-849)

Abstract

Zinc oxide (ZnO) nanoparticles have attracted considerable attention due to their wide bandgap and excellent physicochemical properties, making them promising materials for optoelectronic and photocatalytic applications. However, intrinsic defects such as zinc and oxygen vacancies introduce mid-gap trap states that promote charge carrier recombination, thereby limiting their performance. In this study, ZnO nanoparticles were synthesised via a hydrothermal method and subsequently modified with silver (Ag) nanoparticles through chemical reduction of $AgNO_3$ to enhance light absorption and reduce recombination losses. Structural characterisation using X-ray diffraction (XRD) confirmed the formation of a hexagonal wurtzite ZnO structure with distinct diffraction peaks. Additional diffraction peaks corresponding to metallic Ag indicate successful incorporation of Ag nanoparticles. Optical properties investigated using UV–visible spectroscopy revealed a characteristic absorption band of wurtzite ZnO. Pure ZnO exhibited an absorption peak at 263 nm, while Ag-modified samples showed red-shifted absorption peaks at 264, 270, and 286 nm for increasing Ag concentrations. The enhanced absorption intensity in both UV and visible regions suggests improved light-harvesting capability due to the surface plasmon resonance effect of Ag nanoparticles. Bandgap energies estimated from Tauc plots indicate a reduction in bandgap upon Ag modification, attributed to the introduction of intermediate energy states and plasmonic interactions. The improved optical absorption and bandgap tuning demonstrate that Ag-modified ZnO nanocomposites are promising candidates for enhanced optoelectronic device applications.

Keywords: Zinc oxide (ZnO), red-shift, optoelectronics, silver nanoparticles, hydrothermal synthesis, Optical properties, Bandgap tuning, Surface plasmon resonance

1.0 INTRODUCTION

Zinc oxide (ZnO) is a wide bandgap semiconductor material that exhibits unique electronic and optical properties when at least one dimension is constrained at the nanoscale (Wang, 2004). These properties have found various applications in optics and energy conversion devices. As a result, the study and fabrication of ZnO nanomaterials have been at the forefront of recent research (Xu *et al*., 2012). Some of the important roles played by zinc oxide in the current industry are due to its special characteristics such as anti-corrosion, anti-bacteria and excellent heat resistance. The ZnO nanoparticles are of significant interest as they provide many practical applications worldwide (Heer *et al.,* 2017). Its wide energy band (3.37 eV) and high bond energy (60 meV) make it a good material for application in photoelectronic and electronic devices, devices emitting surface acoustic waves, sensors, field emitters, UV lasers, and dye sensitised solar cells (Agnieszka & Teofil, 2014).

ZnO nanoparticles are synthesised by different methods such as wet chemical method, vapour phase method, hydrothermal method, precipitation method, atomic layer deposition and sonochemical method (Naresh Kumar *et al.,* 2017). The hydrothermal method, unlike other methods, is attributed with the following favourable circumstances, which make it more appropriate and suitable than other methods for ZnO synthesis. The method does not necessitate the use of organic solvents or supplementary processing of the product (grinding and calcination), which makes it a simple and environmentally friendly technique. This synthesis process takes place in an autoclave, where the mixture of substrates is heated slowly to a temperature of 100 –300 °C and left for more than a few days. As a result of heating followed by cooling, crystal nuclei are formed, which then grow. This process has various advantages, including the prospect of carrying out the synthesis at low temperatures, the different shapes and dimensions of the resulting crystals depending on the composition of the starting mixture and the process temperature and pressure (Parihar *et al.,* 2018 & Shivom *et al.,* 2025).

There is a growing need for nanostructured materials with tailored optical and electrical properties. However, a single material does not always provide the required properties: for this reason, a combination of different materials with accurately controlled organisation is

sometimes necessary in order to enhance the performance of a host material and/or to acquire new properties. In this study, ZnO was synthesised and the effect of combining it with noble metal (silver (Ag) plasmon) was investigated by examining the structural and optical properties of the resulting nanocomposite

2.0 EXPERIMENTAL METHOD

2.1 Synthesis of ZnO

In the synthesis of ZnO, 68.145 g of $ZnCl_2$ and 80 g of NaOH which correspond to molar ratio (1:4) was measured respectively using an electronic weighing balance and turned into a beaker containing 100 ml of deionised water. The mixture was stirred continuously until completely dissolved forming a white precipitate of $Zn(OH)_2$. The white precipitate was filtered and washed using deionised water. The filtrate was then dispersed in deionised water and its pH level adjusted to between 11- 12 using hydrochloric acid (HCl) in drops. The pH adjusted mixture was stirred using a magnetic stirrer for 3 hrs and then turned into the Teflon-lining of a hydrothermal autoclave. The solution was heated in a hot air oven at 160 ^oC for 6 hrs. The oven was then allowed to cool to room temperature naturally and the autoclave brought out. The heated mixture was filtered and washed using deionised water. The filtrate was then dried in a hot air oven at 60 ^oC for another 6 hrs. The obtained dry product is the synthesised nanoparticle of ZnO.

2.2 Synthesis of ZnO/Ag nanocomposite

Deposition of Ag on ZnO surface was done as follows: firstly, 500 mg of the as-synthesised white ZnO powder was dispersed well in 20 mL of deionised water using a high-speed dispersant for 30 min. 16.987 mg (0.0001 mol), of the $AgNO_3$ was then added to the above dispersed ZnO solution with continuous stirring so that the $AgNO_3$ is well adsorbed on the ZnO surface. The $AgNO_3$ adsorbed ZnO precipitate was collected and washed several times with deionised water to drain out the excess $AgNO_3$ from the solution. The precipitate was re-dispersed again in 20 mL of deionised water, followed by the addition of 6.41 mg (0.0002 mol) hydrazine hydrate (reducing agent) within the solution with continuous stirring. Ag nanoparticles were deposited onto the surface of ZnO particles, resulting in a yellow-coloured precipitate

3.0 RESULT AND DISCUSSION

3.1 X-Ray Diffraction (XRD)

The X-ray diffraction patterns of the synthesised samples were studied using an X-ray diffractometer (XRD, Rigaku D, Max 2500, Japan) to confirm the crystallinity of the samples and investigate their crystal structure.

Figure 1 shows the XRD patterns of the synthesised ZnO and ZnO/Ag samples deposited on FTO glass substrate by spin coating. As seen in the figure, the ZnO sample revealed eight peaks at various 2theta values.

The synthesised ZnO thin film has the densest plane with the strongest reflection at the (101) plane. It was also observed that the XRD pattern of the ZnO/Ag films has the strongest reflection at (101), the densest plane of the films. Reflections for planes (100), (002), (101), (102), (110), (103), (112) and (201) are also observed for both samples. However, the (111) and (200) planes at 2θ = 38.30and 43.08, respectively, account for the presence of Ag plasmons in the ZnO/Ag samples as Ag grows on the ZnO lattice. Structural changes due to silver doping were not observed.

Useful information that characterises the growth was obtained from the XRD measurement. These include average crystallite size (D), defect density (δ), lattice strain (η), lattice stress (σ), lattice parameters (a, b and c) and d-spacing. The average crystallite size of the nanoparticles was calculated from the Scherrer formula (Jacobsson, 2010).

$$D = \frac{0.94\lambda}{\beta Cos\theta} \qquad (1)$$

where λ is X-ray wavelength (0.15406 nm), β is full width at half maximum (FWHM) and θ is Bragg's diffraction angle.

The dislocation density (δ), which represents the number of defects in the sample, is defined as the length of dislocation lines per unit volume of the crystal. The dislocation density has small values for deposited films, which indicates that microstrains are released due to the thermal annealing. It can be calculated using the equation (Bindu & Thomas, 2014).

$$\delta = \frac{1}{D^2} \qquad (2)$$

Table 1: Crystallite size and defect densities of ZnO and ZnO/Ag samples

Sample	Crystallite size (nm)	Defect densities (nm^{-1})
ZnO	41	$5.95x10^{-4}$
ZnO/Ag1	45	$4.94x10^{-4}$
ZnO/Ag2	39	$6.57x10^{-4}$
ZnO/Ag3	31	$10.4x10^{-4}$

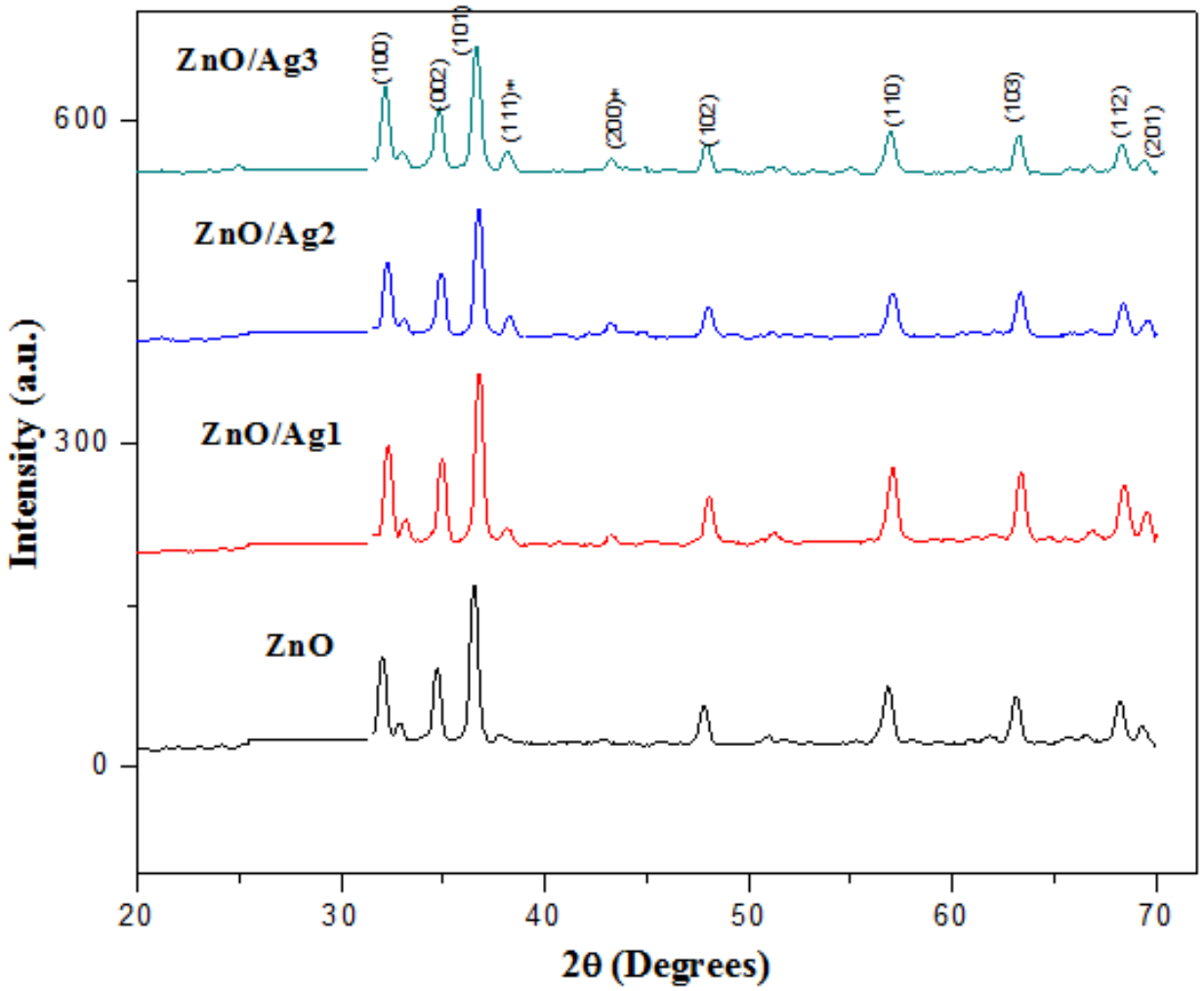

Figure 1: XRD patterns for the as-synthesised ZnO and ZnO/Ag samples.

The calculated crystallite sizes of the as-synthesised ZnO and ZnO/Ag samples are shown in Table 1. It was observed that the crystallite size decreased with increasing concentration of Ag. This occurred as a result of ionic ratio difference between Zn^{2+} and Ag^{+} ions which consequently leads to segregation of Ag at the vicinity of the grain boundary of ZnO. Also, low Ag solubility in ZnO leads to Ag atoms being incorporated in the grain boundaries and/or on the film surface, leading to a reduction in crystallite size. This result complies with what was obtained by Dehimi *et. al.* (2015)

The lattice constants a = b ≠ c and cell volume of the hexagonal structure are obtained using

$$a = b = \frac{\lambda}{\sqrt{3}sin\theta} \quad (3)$$

$$c = \frac{\lambda}{sin\theta} \quad (4)$$

$$V = \frac{\sqrt{3}}{2} \times a^2 c \quad (5)$$

Table 2: Lattice constants and cell volume of the major wurtzite peaks obtained from diffraction patterns of ZnO and ZnO/Ag nanocomposites.

samples	peaks	a = b (Å)	c (Å)	V (Å^3)
ZnO	100	3.22	5.58	50.03
	002	2.98	5.15	39.54
	101	2.84	4.91	34.23
ZnO/Ag1	100	3.19	5.53	48.91
	002	2.96	5.12	38.92
	101	2.82	4.89	33.66
ZnO/Ag2	100	3.20	5.54	49.11
	002	2.96	5.13	39.03
	101	2.82	4.88	33.57
ZnO/Ag3	100	3.21	5.57	49.78
	002	2.97	5.15	39.42
	101	2.83	4.89	33.84

The lattice parameter of a semiconductor depends on the concentration of foreign atoms and defects, external strains and temperature (Ozgur *et al.*, 2005 & Adewale

et al., 2024). Table 2 shows the calculated values of lattice constants and cell volume of the three major peaks of ZnO. The lattice constants of (100) peaks range from 3.19 to 3.22 Å and 5.53 to 5.58 for 'a' and 'c' lattice constants, respectively. These values mostly range from 3.2475 to 3.2501 Å for the 'a' parameter and 5.2042 to 5.2075 Å for the 'c' parameter. The films with 'c' values greater than that of the bulk ZnO value (3.205 Å) have a positive or extensive stress, whereas those with lower values have a negative or compressive stress (Thool *et al.,* 2014).

The lattice strain caused by the substrate and film mismatch, η is evaluated using equation 6

$$\eta = \frac{\beta}{4tan\theta} \qquad (6)$$

The lattice stress in the thin film is calculated using the relation

$$\sigma = -233\frac{c-c_o}{c_o} \qquad (7)$$

where c is the lattice constant of the films and c_o = 5.2066 A^o is the unstrained lattice constant of bulk ZnO. The minus sign indicates the compressive nature of the stress

The interplanar spacing (d) is calculated using Bragg's law, which is given as

$$d = n\lambda sin\theta \qquad (8)$$

where: n is the order of diffraction, λ is the wavelength and θ is the diffraction angle

The interplanar spacing (d_{hkl}) corresponding to the three main peaks calculated using Bragg's law is presented in Table 4. The values are in descending order of magnitude and showed a little deviation from the JCPDS standard values (Gurav *et al.,* 2011).

The percentage contraction is also presented in the same table and lies in the range 0.83-4.5%, with ZnO having the highest contraction value of 4.5%. This suggests that the incorporation of Ag plasmons into ZnO crystals reduced the interplanar spacing contraction of the Ag-doped ZnO nanocomposite.

3.2 Absorption spectra

The optical characterisation was carried out using an ultraviolet–visible light (UV–vis) spectrophotometer (Shimadzu UV-Visible Spectrophotometer, UV-1800 Series, Japan). The optical absorption data were used to evaluate the transmittance, optical bandgap, refractive index, extinction coefficient and other linear and nonlinear optical parameters for the synthesised ZnO and Ag-doped ZnO samples. Figure 2 shows the absorption spectra of both as-synthesised ZnO and Ag-doped ZnO samples. Absorption peaks were observed at 263 nm, 264 nm, 270 nm and 286 nm for ZnO, ZnO/Ag 1, 2 and 3, respectively, which shows a slight shift in absorption peaks. The absorption of the Ag doped ZnO is observed to have high values with Ag concentration increase in the visible region

Transmittance can be calculated from the absorbance result using the Beer-Lambert law. The Beer-Lambert law is the linear relationship between absorbance and concentration of an absorbing species. The law states that the absorbance is proportional to the transmitted intensity (Cosimo, 2015).

$$A = - \log (\% T) \qquad (9)$$

where A is the measured absorbance and T is the transmittance. If equation 4 is expressed in terms of T, it gives (Buba and Adelabu, 2010)

$$T = 10^{-A} \qquad (10)$$

Table 3: Calculated structural parameters of the three major peaks for ZnO and Ag-doped ZnO

Samples	Peak position(°)	β (Radians)	$\eta \times 10^{-3}$	σ (Gpa)
ZnO	32.081	0.1968	2.987	-2598.89
	34.780	0.1574	2.193	-2830.05
	36.509	0.2362	2.989	-3108.16
ZnO/Ag1	32.3313	0.1968	2.962	-2243.27
	34.9698	0.1574	2.18	-2061.63
	36.7637	0.1181	1.551	-1953.26
ZnO/Ag2	32.2863	0.1968	2.967	-2246.63
	34.935	0.1968	2.729	-2063.85
	36.7987	0.2362	3.098	-1951.25
ZnO/Ag3	32.1363	0.2755	4.173	-2257.9
	34.8154	0.2362	3.287	-2071.49
	36.696	0.2755	3.625	-1957.15

.Table 4 Interplanar spacing (d_{hkl}) from XRD, JCPDS data card for corresponding (hkl) values and percentage variation of d.

Sample	Hkl	d_{XRD} (Å)	d_{JCPDS} (Å)	Contraction (%)
ZnO	100	2.79004	2.8135	0.833837
	002	2.57945	2.6027	0.893303
	101	2.36471	2.4751	4.460022
ZnO/Ag1	100	2.76902	2.8135	1.580949
	002	2.5659	2.6027	1.413916
	101	2.44472	2.4751	1.227425
ZnO/Ag2	100	2.77277	2.8135	1.447663
	002	2.56838	2.6027	1.318631
	101	2.44247	2.4751	1.318331
ZnO/Ag3	100	2.78537	2.8135	0.999822
	002	2.57693	2.6027	0.990126
	101	2.44907	2.4751	1.051675

Figure 3 shows the transmittance plot against wavelength for the as-synthesised ZnO and ZnO/Ag samples.

The transmittance of the as-synthesised ZnO and ZnO/Ag samples was observed in the spectral range of 280-900 nm as seen in Figure 3. The pure as-synthesised ZnO oxide exhibited a transmittance of 83%, making it a good window material for optoelectronic applications. A transmittance value of 74%, 70% and64% was observed for ZnO/Ag1, ZnO/Ag2 and ZnO/Ag3 samples, respectively. An increase in scattering due to the roughness of the surface of nanoparticles and oxygen vacancies produces a decrease in optical transmission (Kayani *et al.,* 2020). This trend was observed in a research work by Suman *et al*. (2013).

The extinction coefficient describes the attenuation of light in a medium and a higher *k* value indicates the probability of raising the electron transfer across the mobility gap with photon energy. Therefore, the higher values represent greater attenuation of light in a thin film (Hossain *et al.,* 2018). It is mathematically expressed as (Abdelraheem *et al*., 2020)

$$k = \frac{\alpha\lambda}{4\pi} \qquad (11)$$

α is the absorption coefficient, λ is the wavelength.

Figure 4 shows the extinction coefficient (*k*) spectra of the ZnO and Ag-doped ZnO thin films. It is observed that the extinction coefficient falls abruptly with the increase of wavelength in the UV region. Higher values were observed in the visible spectra region.

In modern-day optoelectronics and its design, the knowledge of refractive index variation with wavelength is useful in predicting the photoelectric characteristics of a device (Ostroverkhova & Singer, 2002). The refractive index was evaluated using the relation

$$n = \frac{(1+R)}{(1-R)} + \left[\frac{4R}{(1-R)^2} - K^2\right]^{1/2} \qquad (12)$$

where R is reflectance obtained from the unity equation and k is the extinction coefficient. Figure 4 shows a plot of refractive index versus wavelength for the as-synthesised ZnO and Ag samples. The refractive index's highest peak was observed in the UV region, later accompanied by an exponential decrease. The reduction in refractive index with wavelength depicts the dependence correlation between absorption coefficient and refractive index, which indicates the normal behaviour of the as-synthesised ZnO and ZnO/Ag samples. This is in accordance with the studies by Ahmad *et al*. (2019, Kumar *et. al*. (2016 & Kumar *et al. (*2024).

The numerical values of the refractive index between 300-900 nm wavelength is observed to be higher with the addition of Ag content. This may be attributed to the increase in polarisability. The atomic radius of Ag is larger than that of Zn. The longer the atomic radius, the larger the polarisability as explained by the Lorentz-Lorenz equation (Shaaban *et al.,* 2016)

The optical conductivity of the material was also estimated using equation (13).

$$\sigma = \frac{\alpha nc}{4\pi k} \qquad (13)$$

where α, n, c and k are the absorption coefficient, refractive index, speed of light and extinction coefficient, respectively. Figure 6 shows a plot of optical conductivity for the as-synthesised ZnO and ZnO/Ag samples. The optical conductivity measures the number of free charges present in the material (Chen *et al.,* 2024 & Rosowska *et al.,* 2025). The free carriers increase in ZnO/Ag nanocomposite with Ag content. The enhancement in optical conductivity is high in the high-energy region (UV), because free carriers absorb photon energy. While the decrement in the optical conductivity in the visible region is due to trapping of free carriers (Kayani *et al.,* 2020).

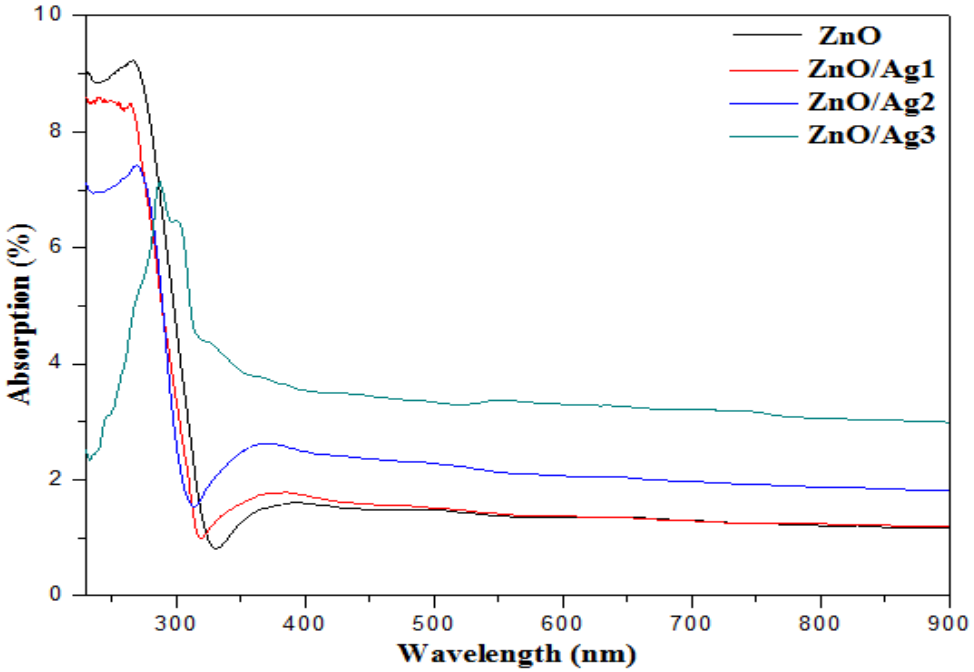

Figure 2: (a) Absorption spectra of as-synthesised ZnO and ZnO/Ag

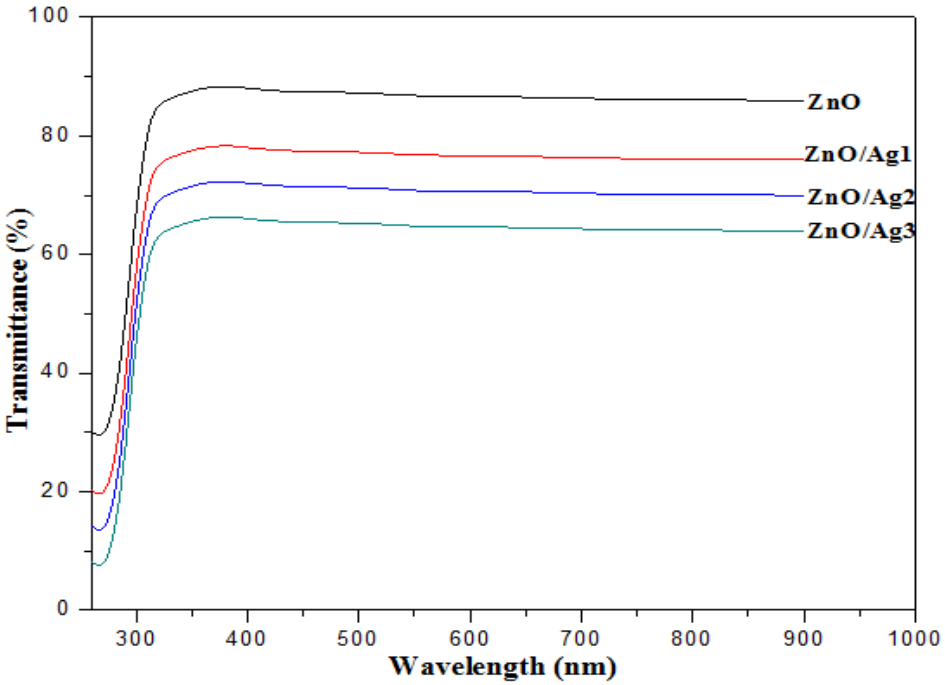

Figure 3: Transmittance spectra of the as-synthesised ZnO and ZnO/Ag samples.

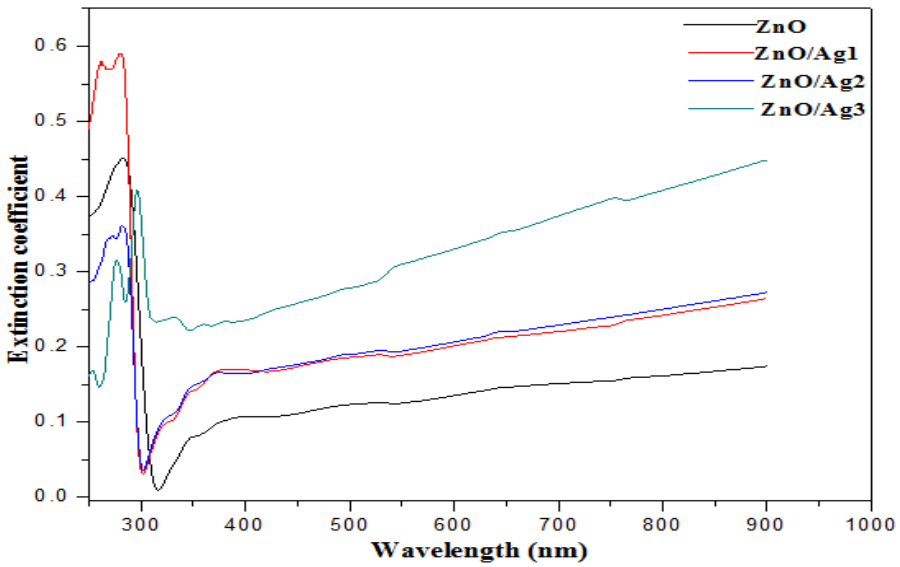

Figure 4: A plot of extinction coefficient against photon energy for the as-synthesised ZnO and ZnO/Ag samples.

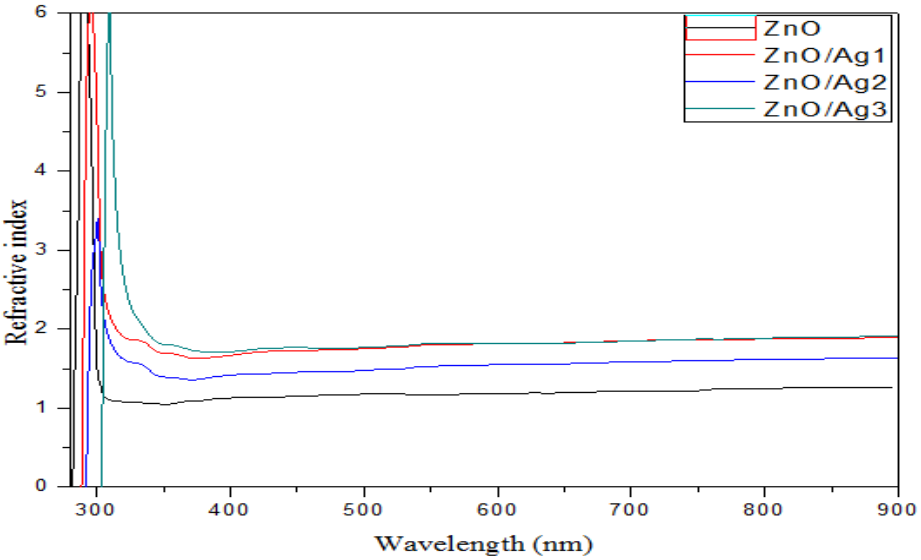

Figure 5: A plot of refractive index versus wavelength for the synthesised ZnO and ZnO/Ag samples

3.3 Optical bandgap

The optical energy band gap was calculated using Tauc's formula given as:

$$(\alpha h\nu)^n = k\left(h\nu - E_g\right) \quad (14)$$

where α is the absorption coefficient, h is Planck's constant, ν is the photon energy, and k is the band tailing parameter (constant). Figure 7(a-d) shows the plot of $(\alpha h\nu)^2$ versus photon energy for the as-synthesised ZnO and ZnO/Ag samples. The band gap extrapolated for the synthesised ZnO and Ag-doped ZnO is presented in Table 5. It was observed that the band gap energy decreased with increasing concentration of Ag. This is due to the creation of intermediate states between the conduction and valence bands of ZnO host matrix with the addition of Ag, which are responsible for the reduction in the calculated band gap of ZnO/Ag samples. Ag plays the role of acceptor material to change the band gap of the as-synthesised ZnO and hence, decrease the band gap (Kumar *et. al*., 2016).

Table 5: Optical bandgap values for ZnO and ZnO/Ag samples.

S/No	Compound	Bandgap energy (eV)
1	ZnO	3.49
2	ZnO/Ag1	3.35
3	ZnO/Ag2	3.26
4	ZnO/Ag3	3.13

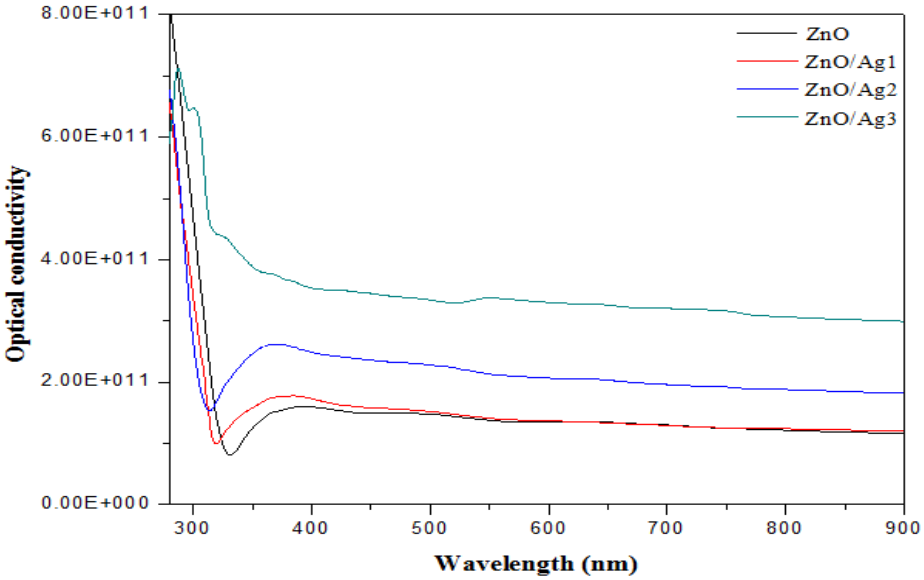

Figure 6: A plot of optical conductivity against photon energy for the as-synthesised ZnO and ZnO/Ag samples.

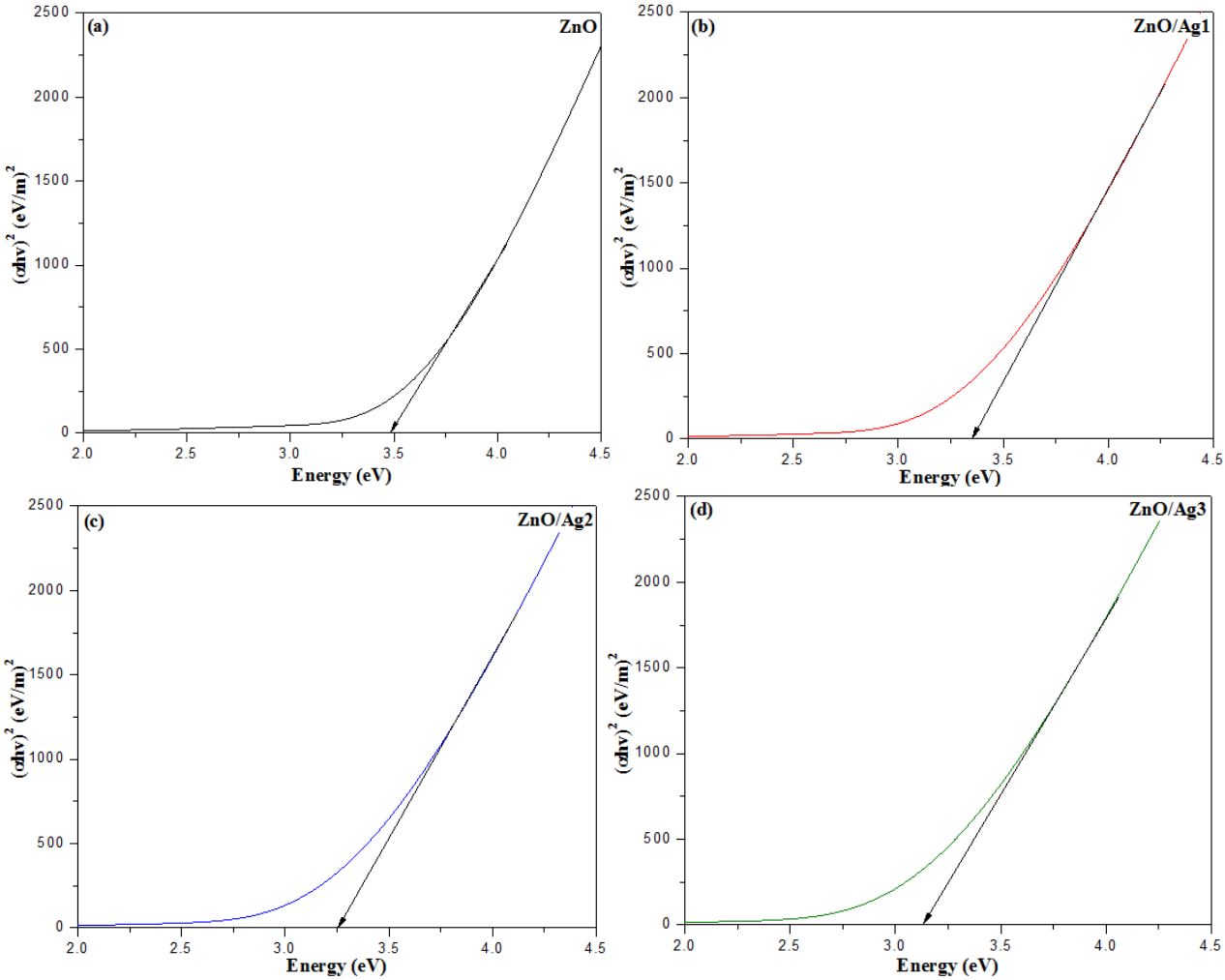

Figure 7(a-d): Plot of optical bandgap versus photon energy for the as-synthesised ZnO and ZnO/Ag samples.

4.0 CONCLUSION

In conclusion, ZnO has been synthesised via the hydrothermal method. The as-synthesised ZnO was doped with Ag plasmons by the reduction of $AgNO_3$ to Ag ions using hydrazine hydrate as reducing agent in order to enhance the photon absorption of ZnO in the visible spectrum region of light spectra. XRD pattern corresponding to (100), (002) and (101) planes, which identify the wurtzite ZnO, was revealed. An additional peak observed at 2θ values of 38.3 ° and 43.08 ° corresponds with silver (111) and (200) planes, respectively. A right-hand shift to a higher wavelength attributed to the presence of Ag plasmons in the ZnO lattice was observed for Ag-doped samples. ZnO/Ag_3 has the highest absorption range of 365 nm and 430 nm in the UV-visible spectra. The refractive index plots are in accordance with the standard for both doped and undoped ZnO. The increase in refractive index with Ag addition has been explained in terms of polarisability. The band gap values obtained from Tauc's plots reveal the energy level in between the conduction and valence bands of the synthesised wide bandgap of the synthesised photocatalyst. The Wigner distribution deconvolution (WDD) model was used to calculate and interpret the optoelectronic and dispersion properties of ZnO and Ag-doped ZnO thin films. A composite of oxide thin films with controllable refractive index and tunable optical and optoelectronic properties provides a pathway to design smart multi-functional materials. Such materials may act as potential candidates for the fabrication of modern optoelectronic devices and thin-film transistors.

REFERENCES

Abdelraheem, A. M., Abd-Elrahman, M. I., Mohamed, M., Hadia, N. M. A., & Shaaban, E. R. (2020). Linear and non-linear optical parameters of diluted magnetic semiconductor CdS0. 9Mn0. 1 thin film: influence of the film thickness. *Journal of Electronic Materials*, *49*(3), 1944-1956.

Agnieszka, K. & Teofil, J. (2014). Zinc oxide -from synthesis to application: a review. Materials 2833-2881. doi: 10.3390/ma7042833.

Ahmad, I., Ahmed, E., & Ahmad, M. (2019). The excellent photocatalytic performances of silver-doped ZnO nanoparticles for hydrogen evolution. *SN Applied Sciences*, *1*(4), 1-12.

Adewale, A. T., Zhang, Y., & Li, X. (2024). Enhanced ultraviolet photodetection with Ag nanoparticle-decorated ZnO nanowires. *Optical Materials, 147, 114563. https://doi.org/10.1016/j.optmat.2024.114563*

Bindu, P., & Thomas, S. (2014). Estimation of lattice strain in ZnO nanoparticles: X-ray peak profile analysis. *Journal of Theoretical and Applied Physics*, *8*(4), 123-134.

Buba, A. D. A., & Adelabu, J. S. A. (2010). Optical and electrical properties of chemically deposited ZnO thin films. *The Pacific Journal of Science and Technology*, *11*(2), 429-434.

Chen, H., Kumar, R., & Singh, M. (2024). Silver nanogranules-decorated ZnO hybrid nanostructures with enhanced UV photoresponses. *Materials Today Communications, 39, 108247. https://doi.org/10.1016/j.mtcomm.2024.108247*

Cosimo, D. C. and Claudia, H. (2015). UV/VIS Spectrophotometry - Fundamentals and Applications. Mettler-Toledo Publication No. ME-30256131.

Dehimi, M., Touam, T., Chelouche, A., Boudjouan, F., Djouadi, D., Solard, J., ... & Doghmane, A. (2015). Effects of low Ag doping on physical and optical waveguide properties of highly oriented sol-gel ZnO thin films. *Advances in Condensed Matter Physics*, *2015*.

Gurav, K. V., Patil, U. M., Pawar, S. M., Kim, J. H., & Lokhande, C. D. (2011). Controlled crystallite orientation in ZnO nanorods prepared by chemical bath deposition: Effect of H2O2. *Journal of alloys and compounds*, *509*(29), 7723-7728.

Heer, A. S. K., Mansoori, S. M. and Chamria, N. (2017). Biosynthesis and Characterization of Zinc Oxide Nanoparticle Using Ficus Religiosa Leaves Extract, World Journal of Pharmaceutical Research Volume 6, Issue 10, 818-826.

Hossain, S., Quaderi, G. D. A., Hussain, K. M. A., & Faruqe, T. (2018). Synthesis and Characterization of Undoped and Aluminum Doped Zinc Oxide Thin Films using Thermal Evaporation Method. *NUCLEAR SCIENCE AND APPLICATIONS*, *27*(1&2).

Jacobsson, T. J. (2010). Synthesis and characterisation of ZnO nanoparticles. An experimental investigation of some of their size dependent quantum effects.

Kayani, Z. N., Manzoor, F., Zafar, A., Mahmood, M., Rasheed, M., & Anwar, M. (2020). Impact of Ag doping on structural, optical, morphological, optical and photoluminescent properties of ZnO nanoparticles. *Optical and Quantum Electronics*, *52*(7), 1-18.

Kumar, S., Verma, A., & Sharma, P. (2024). Structural, optical, and photocatalytic properties of Ag/Cu-decorated ZnO nanoparticles. *Journal of Materials Science*: *Materials in Electronics,*

35(12), 10234–10245. https://doi.org/10.1007/s10854-024-12919-4

Kumar, S., Singh, V., & Tanwar, A. (2016). Structural, morphological, optical and photocatalytic properties of Ag-doped ZnO nanoparticles. *Journal of Materials Science: Materials in Electronics*, *27*(2), 2166-2173

Naresh Kumar, P., Sakthivel, K., & Balasubramanian, V. (2017). Microwave assisted biosynthesis of rice shaped ZnO nanoparticles using Amorphophallus konjac tuber extract and its application in dye sensitized solar cells, *Materials Science-Poland*, *35*(1), 111-119. doi: https://doi.org/10.1515/msp-2017-0029

Ostroverkhova, O., & Singer, K. D. (2002). Space-charge dynamics in photorefractive polymers. *Journal of applied physics*, *92*(4), 1727-1743.

Özgür, Ü., Alivov, Y. I., Liu, C., Teke, A., Reshchikov, M., Doğan, S., ... & Morkoç, A. H. (2005). A comprehensive review of ZnO materials and devices. *Journal of applied physics*, *98*(4), 11.

Parihar, V., Raja, M., & Paulose, R. (2018). A brief review of structural, electrical and electrochemical properties of zinc oxide nanoparticles. Reviews on Advanced Materials Science, 53(2), 119-130.

Rosowska, J., Kaczmarek, D., & Nowak, P. (2025). Influence of precursor chemistry on structural and optical properties of ZnO nanoparticles synthesized via microwave-assisted hydrothermal method. *Nanomaterials, 15(3), 230. https://doi.org/10.3390/nano15030230*

Shaaban, E. R., El-Hagary, M., Moustafa, E. S., Hassan, H. S., Ismail, Y. A., Emam-Ismail, M., & Ali, A. S. (2016). Structural, linear and nonlinear optical properties of co-doped ZnO thin films. *Applied Physics A*, *122*(1), 1-10.

Suman, T.Y., Rajasree, S.R.R., Kanchana, A., & Elizabeth, S.B. (2013). Biosynthesis, characterization and cytotoxic effect of plant mediated silver nanoparticles using Morinda citrifolia root extract. *Colloids and surface B: Biointerfaces*, 106, 74 – 78.

Shivom, S., Gupta, R., & Tiwari, P. (2025). Design of Ag-decorated ZnO nanoflakes for efficient photodegradation of pharmaceutical pollutants under solar irradiation. *Materials Today Sustainability. https://doi.org/10.1016/j.*

Thool, G. S., Singh, A. K., Singh, R. S., Gupta, A., & Susan, M. A. B. H. (2014). Facile synthesis of flat crystal ZnO thin films by solution growth method: a micro-structural investigation. *Journal of Saudi Chemical Society*, *18*(5), 712-721.

Wang, Z. L. (2004). Zinc oxide nanostructures: growth, properties and applications. J. Phys.: Condens. Matter 16 R829–R858 doi:10.1088/0953-8984/16/25/R01

Xu, X., Wu, M., Asoro, M., Ferreira, P. J., & Fan, D. L. (2012). One-Step Hydrothermal Synthesis of Comb-Like ZnO Nanostructures. Crystal growth & design, 12(10), 4829–4833. https://doi.org/10.1021/cg3005773